Thermal Conductivity in the Boundary Layer of Non-Newtonian Fluid with Particle Suspension

Rudraswamy N.G., Ganeshkumar K.,
Krishnamurthy M.R., Gireesha B.J. and Venkatesh P.

Additional information is available at the end of the chapter

Abstract

The present chapter is focused on studies concerned with three-dimensional flow and heat transfer analysis of Carreau fluid with nanoparticle suspension. The heat transfer analysis in the boundary was carried out with the fluid flow over a stretching surface under the influence of nonlinear thermal radiation, mixed convection and convective boundary condition. Suitable similarity transformations are employed to reduce the governing partial differential equations into coupled nonlinear ordinary differential equations. The equations in non-linear form are then solved numerically using Runge-Kutta-Fehlberg fourth fifth-order method with the help of symbolic algebraic software MAPLE. The results so extracted are well tabulated and adequate discussions on the parameters affecting flow and heat transfer analysis were carried out with the help of plotted graphs.

Keywords: Carreau nano fluid, nonlinear thermal radiation, mixed convection, stretching sheet, convective boundary condition, numerical method

1. Introduction

Thermal radiation, the fundamental mechanism of heat transfer is an indispensable activity in rocket propulsion, plume dynamics, solar collector performance, materials processing, combustion systems, fire propagation and other industrial and technological processes at high temperatures. With the developments in computational dynamics, increasing attention has been diverted towards thermal convection flows with the significant radiative flux. Rayleigh initiated the theory of thermal convection, by deriving critical temperature gradient (Critical Rayleigh number). Importance of such radiations is intensified with absolute temperatures at

higher level. Thus a substantial interest is driven towards thermal boundary layer flows with a strong radiation. Governing equation of radiative heat transfer with its integro-differential nature makes numerical solutions of coupled radiative-convective flows even more challenging. Multiple studies were conducted employing several models to investigate heat and mass transfer in boundary layer and fully-developed laminar convection flows. As a consequence several simultaneous multi-physical effects in addition to radiative heat transfer including gravity and pressure gradient effects [1], mhd flow of nanofluids [2], buoyancy effects [3, 4], ferrofluid dynamics [5], stretching surface flow [6, 7], time-dependent, wall injection and Soret/Dufour effects [8–11].

These studies have however been confined to Newtonian flows. But industries related with fabrication of polymers and plastics at high temperatures show greater importance towards radiative flows of non-Newtonian fluids. The potential of non-Newtonian flows in ducts with radiative transfer were significantly developed after the studies on novel propellants for spacecraft [12]. The developments are extant and diversified the application of non-Newtonian fluid models. Most studies in this regard have employed the Rosseland model which is generally valid for optically-thick boundary layers. Recently, Kumar et al. [13] used such model to study melting heat transfer of hyperbolic tangent fluid over a stretching sheet with suspended dust particles. Cortell [14] and Batalle [15] have shown their earlier contribution towards radiative heat transfer of non-Newtonian fluids past stretching sheet under various circumstances. Relating to the studies Khan et al. [16] developed a numerical studies correlating MHD flow of Carreau fluid over a convectively heated surface with non-linear radiation. Appending to this studies Khan et al. [17] provided his results on hydromagnetic nonlinear thermally radiative nanoliquid flow with Newtonian heat along with mass conditions. Meanwhile, Rana and Bhargava [18] provided a numerical elucidation to study of heat transfer enhancement in mixed convection flow along a vertical plate with heat source/sink utilizing nanofluids. Hayat et al. [19] investigated the mixed convection stagnation-point flow of an incompressible non-Newtonian fluid over a stretching sheet under convective boundary conditions. Many diverse -physical simulations with and without convective and/or radiative heat transfer have been studied. Representative studies in this regard include [20–23] with analogous to the property of radiation flow.

Endeavoring the complications in three dimensional flow analysis, Shehzad et al. [24] studied the effect of thermal radiation in Jeffrey nanofluid by considering the characteristics of thermophoresis and Brownian motion for a solar energy model. Hayat et al. [25] analyzed the effect non-linear thermal radiation over MHD three-dimensional flow of couple stress nanofluid in the presence of thermophoresis and Brownian motion. Rudraswamy et al. [26] observations on Soret and Dufour effects in three-dimensional flow of Jeffery nanofluid in the presence of nonlinear thermal radiation clearly showed that concentration and associated boundary layer thickness are enhanced by increasing Soret and Dufour numbers. Many such problems [27–29] were considered disclosing the feature of thermal radiation in three dimensional flow of non-Newtonian fluids.

Inspired by the above works, we put forth the studies on the effect of non-linear thermal radiation on three dimensional flow of Carreau fluid with suspended nanoparticles. Present

studies even include the phenomenon of mixed convection and convective boundary conditions. A numerical approach is provided for the above flow problem by employing Runge-Kutta-fourth-fifth order method.

2. Mathematical formulation

A steady three-dimensional flow of an incompressible Carreau fluid with suspended nano particles induced by bidirectional stretching surface at $z = 0$ has been considered. The sheet is aligned with the $xy-$ plane $(z = 0)$ and the flow takes place in the domain $z > 0$. Let $u = u_w(x) = ax$ and $v = v_w(y) = by$ be the velocities of the stretching sheet along x and y directions respectively. A constant magnetic field of strength B is applied in the $z-$ direction. Heat and mass transfer characteristics are taken in to account in the presence of Brownian motion and Thermophoresis effect. The thermo physical properties of fluid are taken to be constant.

Extra stress tensor for Carreau fluid is.

$$\overline{\tau}_{ij} = \mu_0 \left[1 + \frac{n-1}{2} \left(\Gamma \overline{\gamma} \right)^2 \right] \overline{\gamma}_{ij}$$

In which $\overline{\tau}_{ij}$ is the extra stress tensor, μ_0 is the zero shear rate viscosity, Γ is the time constant, $\overline{\gamma}$ is the power law index and is defined as.

$$\overline{\gamma} = \sqrt{\frac{1}{2} \sum \sum \overline{\gamma}_{ij} \overline{\gamma}_{ji}} = \sqrt{\frac{1}{2} \Pi}$$

Here Π is the second invariant strain tensor.

The governing boundary layer equations of momentum, energy and concentration for three-dimensional flow of Carreau nanofluid can be written as,

$$\frac{\partial u}{\partial x} + \frac{\partial v}{\partial y} + \frac{\partial w}{\partial z} = 0, \tag{1}$$

$$u \frac{\partial u}{\partial x} + v \frac{\partial u}{\partial y} + w \frac{\partial u}{\partial z} = v \frac{\partial^2 u}{\partial z^2} + 3 \frac{(n-1)}{2} \Gamma \left(\frac{\partial u}{\partial z} \right)^2 \frac{\partial^2 u}{\partial z^2} + g \beta_T (T - T_\infty) - \frac{\sigma B^2}{\rho} u, \tag{2}$$

$$u \frac{\partial v}{\partial x} + v \frac{\partial v}{\partial y} + w \frac{\partial v}{\partial z} = v \frac{\partial^2 v}{\partial z^2} + 3 \frac{(n-1)}{2} \Gamma \left(\frac{\partial v}{\partial z} \right)^2 \frac{\partial^2 v}{\partial z^2} - \frac{\sigma B^2}{\rho} v, \tag{3}$$

$$u \frac{\partial T}{\partial x} + v \frac{\partial T}{\partial y} + w \frac{\partial T}{\partial z} = \alpha \frac{\partial^2 T}{\partial z^2} + \tau \left[D_B \frac{\partial T}{\partial z} \frac{\partial C}{\partial z} + \frac{D_T}{T_\infty} \left(\frac{\partial T}{\partial z} \right)^2 \right] - \frac{1}{(\rho c)_f} \frac{\partial q_r}{\partial z}, \tag{4}$$

$$u \frac{\partial C}{\partial x} + v \frac{\partial C}{\partial y} + w \frac{\partial C}{\partial z} = D_B \frac{\partial^2 C}{\partial z^2} + \frac{D_T}{T_\infty} \frac{\partial^2 T}{\partial z^2}. \tag{5}$$

The boundary conditions for the present flow analysis are,

$$u = ax, v = by, w = 0, k\frac{\partial T}{\partial z} = -h_f(T_f - T_\infty), C = C_w \text{ at } z = 0 \tag{6}$$

$$u \to 0, v \to 0, T \to T_\infty, C \to C_\infty \text{ as } z \to \infty, \tag{7}$$

where v is the kinematic viscosity of the fluid, μ is the coefficient of fluid viscosity, ρ is the fluid density, B is the magnetic field, σ is the electrical conductivity of the fluid, T is the fluid temperature, α is the thermal diffusivity of the fluid, k is the thermal conductivity. τ is the ratio of effective heat capacity of the nanoparticle material to heat capacity of the fluid, q_r is the radiative heat flux, g is the gravitational acceleration, β_T is thermal expansion coefficient of temperature, D_B is the Brownian diffusion coefficient, h_f is the heat transfer coefficient, D_T is the thermophoretic diffusion coefficient, c_p is the specific heat at constant pressure, T_f is the temperature at the wall, T_∞ is the temperatures far away from the surface. C is the concentration and C_∞ is the concentration far away from the surface. The subscript w denotes the wall condition.

Using the Rosseland approximation radiation heat flux q_r is simplified as,

$$q_r = -\frac{4\sigma^*}{3k^*}\frac{\partial T^4}{\partial z} = -\frac{16\sigma^*}{3k^*}T^3\frac{dT}{dz}, \tag{8}$$

where σ^* and k^* are the Stefan-Boltzmann constant and the mean absorption coefficient respectively.

In view to Eq. (8), Eq. (4) reduces to.

$$u\frac{\partial T}{\partial x} + v\frac{\partial T}{\partial y} + w\frac{\partial T}{\partial z} = \frac{\partial}{\partial z}\left[\left(\alpha + \frac{16\sigma^*T^3}{3k^*(\rho c)_f}\right)\frac{dT}{dz}\right] + \tau\left[D_B\frac{\partial T}{\partial z}\frac{\partial C}{\partial z} + \frac{D_T}{T_\infty}\left(\frac{\partial T}{\partial z}\right)^2\right]. \tag{9}$$

The momentum, energy and concentration equations can be transformed into the corresponding ordinary differential equations by the following similarity variables,

$$u = axf'(\eta), v = byg'(\eta), w = -\sqrt{av}(f(\eta) + g(\eta)),$$

$$\theta(\eta) = \frac{T - T_\infty}{T_w - T_\infty}, \phi(\eta) = \frac{C - C_\infty}{C_w - C_\infty}, \eta = \sqrt{\frac{a}{v}} \tag{10}$$

where $T = T_\infty(1 + (\theta_w - 1)\theta(\eta))$, $\theta_w = \frac{T_f}{T_\infty}$, $(\theta_w > 1)$ being the temperature ratio parameter.

Then, we can see that Eq. (1) is automatically satisfied, and Eqs. (2)–(7) are reduced to:

$$f''' + (f + g)f'' - f'^2 + 3\frac{n-1}{2}Wef''^2f''' + \lambda\theta - Mf' = 0 \tag{11}$$

$$g''' + (f + g)g'' - g'^2 + 3\frac{n-1}{2}Weg''^2g''' - Mg' = 0 \tag{12}$$

$$\frac{1}{\Pr}\left((1 + R(\theta_w - 1)\theta)^3\theta''\right) + (f + g)\theta' + Nb\theta'\varphi' + Nt\theta'^2 = 0, \tag{13}$$

$$\phi'' + Le\Pr(f + g)\phi' + \frac{Nt}{Nb}\theta'' = 0 \tag{14}$$

With the boundary conditions,

$$f = 0, g = 0, f' = 1, g' = c, \theta' = -Bi(1 - \theta(0)), \quad \phi = 1, \quad \text{at } \eta = 0,$$

$$f' \to 0, g' \to 0, \theta \to 0, \phi \to 0 \text{ as } \eta \to \infty. \tag{15}$$

$We = \frac{cU_w^2\lambda^2}{\nu}$ is the Weissenberg number, $M = \frac{\sigma B^2}{\rho a}$ is the magnetic parameter, $c = \frac{b}{a}$ is the ratio of stretching rates, $\Pr = \frac{\nu}{\alpha}$ is Prandtl number, $R = \frac{16\sigma^* T_\infty^3}{3kk^*}$ is the radiation parameter, $Nb = \frac{\tau D_B(C_w - C_\infty)}{\nu}$ is the Brownian motion parameter, $Nt = \frac{\tau D_T(T_f - T_\infty)}{\nu T_\infty}$ is the Thermophoresis parameter, $\lambda = \frac{g\beta_T(T_f - T_\infty)}{\Re_x}$ is the mixed convection parameter, $Bi = \frac{h_f}{k}\sqrt{\frac{\nu}{a}}$ is the Biot number, $Le = \frac{\alpha}{D_B}$ is the Lewis number.

The local skin friction (C_f), local Nusselt number (Nu_x) and local number Sherwood (Sh_x) are defined as,

$$C_{fx} = \frac{\tau_w}{\rho u_w(x)^2}, C_{fy} = \frac{\tau_w}{\rho v_w(y)^2}, Nu_x = \frac{u_w q_w}{ka(T_f - T_\infty)} \text{ and } Sh_x = \frac{u_w q_m}{D_B a(C_w - C_\infty)}$$

The local skin friction, local Nusselt number and Sherwood number is given by,

$$\sqrt{\Re_x}C_{fx} = \left[f''(0) + \frac{(n-1)We^2}{2}\left(f''(0)\right)^3\right], \quad \sqrt{\Re_x}C_{fy} = \left[g''(0) + \frac{(n-1)We^2}{2}\left(g''(0)\right)^3\right],$$

$$\frac{Nu_x}{\sqrt{\Re_x}} = -\left(1 + +R\theta_w^3\right)\theta'(0), \quad \frac{Sh_x}{\sqrt{\Re_x}} = -\phi'(0).$$

where $\Re_x = \frac{u_w x}{\nu}$ is the local Reynolds number based on the stretching velocity. $u_w(x)$.

3. Numerical method

The non-linear ordinary differential Eqs. (11)–(14) subjected to boundary conditions (15) has been solved using the Runge-Kutta-Fehlberg fourth-fifth order method with the help of symbolic algebraic software MAPLE. The boundary conditions for $\eta = \infty$ are replaced by $f'(\eta_{max}) = 1, \theta(\eta_{max}) = 0$ and $\phi(\eta_{max}) = 0$, where η_{max} is a sufficiently large value of η at which the boundary conditions (15) are satisfied. Thus, the values of $\eta = \eta_{max}$ are taken to be 6. To validate the employed method, the authors have compared the results of $f''(0)$ and $g''(0)$

c	Wang [27]		Hayat et al. [30]		Present result	
	$-f''(0)$	$-g''(0)$	$-f''(0)$	$-g''(0)$	$-f''(0)$	$-g''(0)$
0	1	0	1	0	1	0
0.25	1.0488	0.1945	1.048810	0.19457	1.04881	0.19457
0.5	1.0930	0.4652	1.093095	0.465205	1.09309	0.46522
0.75	1.1344	0.7946	1.134500	0.794620	1.13450	0.79462
1.0	1.1737	1.1737	1.173721	1.173721	1.17372	1.17372

Table 1. Comparison of different values of c with Wang [27] and Hayat et al. [30].

with the that of published works by Wang [27] and Hayat [30] for the different values stretching parameter. These comparisons are given in **Table 1** and it shows that the results are in very good agreement.

4. Result and discussion

The purpose of this section is to analyze the effects of various physical parameters on the velocities, temperature and concentration fields. Therefore, for such objective, **Figures 1–11** has been plotted. Observations over these data with plotted graphs are discussed below.
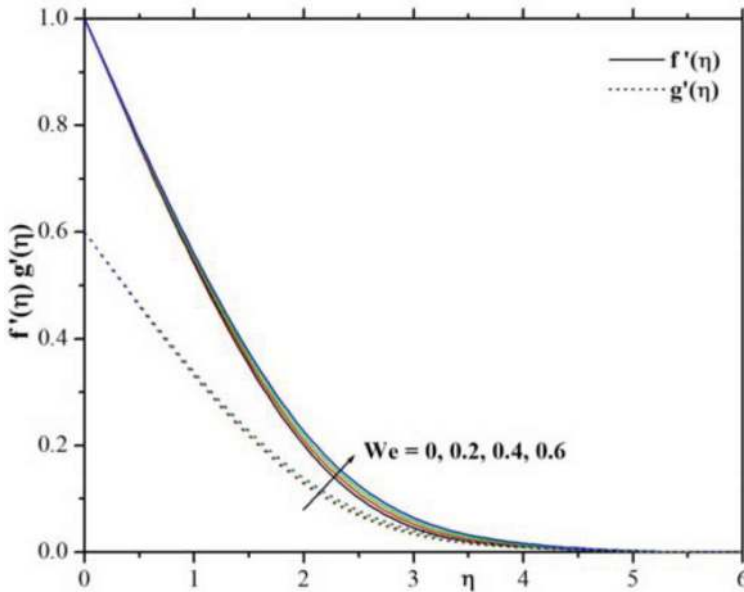
Figure 1. Influence of *We* on velocity profiles of both $f'(\eta)$ and $g'(\eta)$.
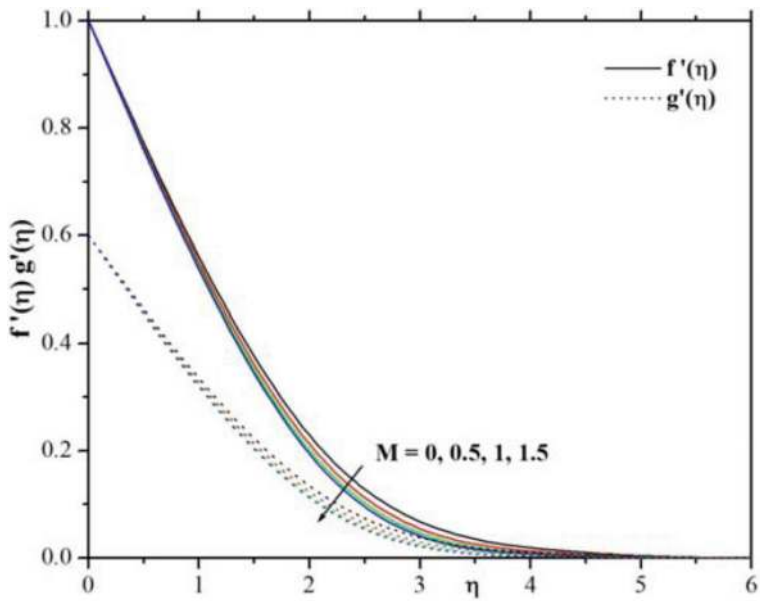
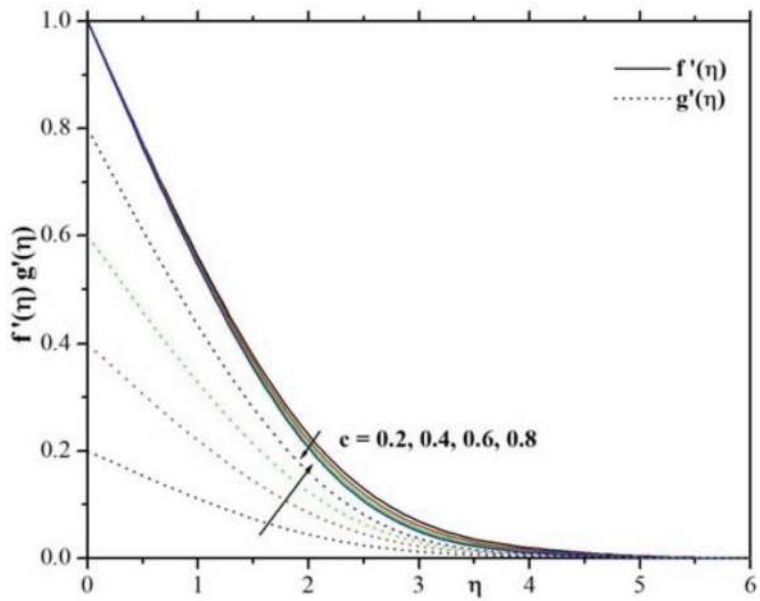**Figure 2.** Influence of M on velocity profiles $f'(\eta)$ and $g'(\eta)$.

Figure 3. Influence of c on velocity profiles $f'(\eta)$ and $g'(\eta)$.
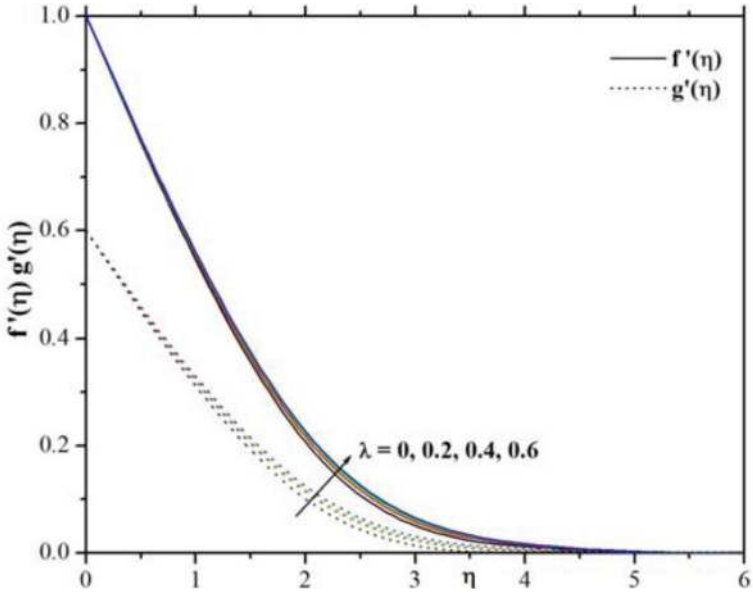
Figure 4. Influence of λ on velocity profiles $f'(\eta)$ and $g'(\eta)$.
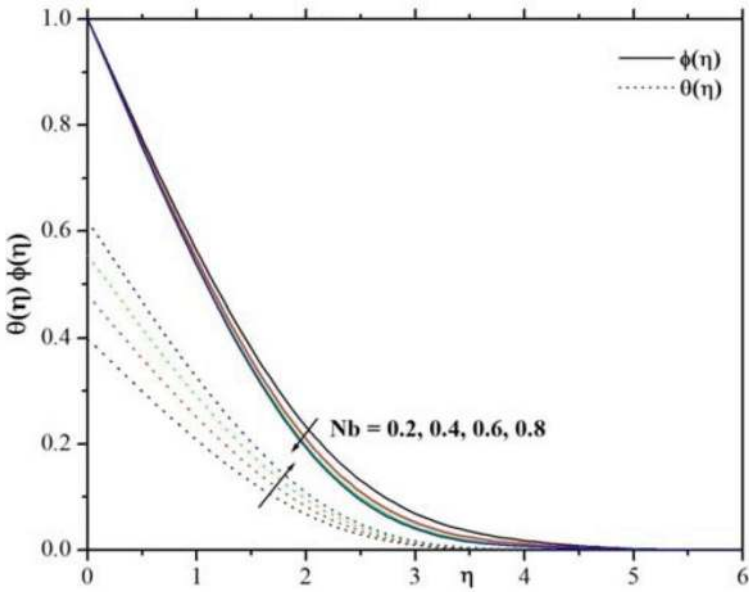

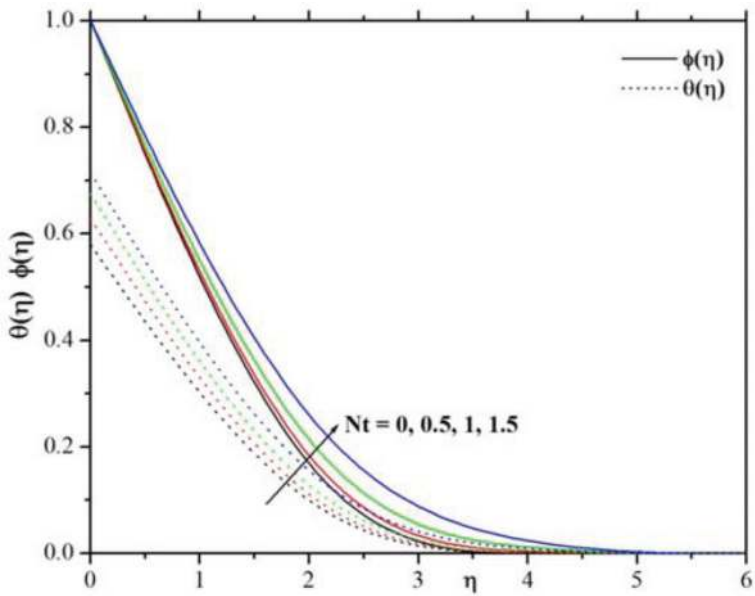**Figure 5.** Influence of Nb on $\theta(\eta)$ and $\phi(\eta)$ profiles.

Figure 6. Influence of Nt on $\theta(\eta)$ and $\phi(\eta)$ profiles.
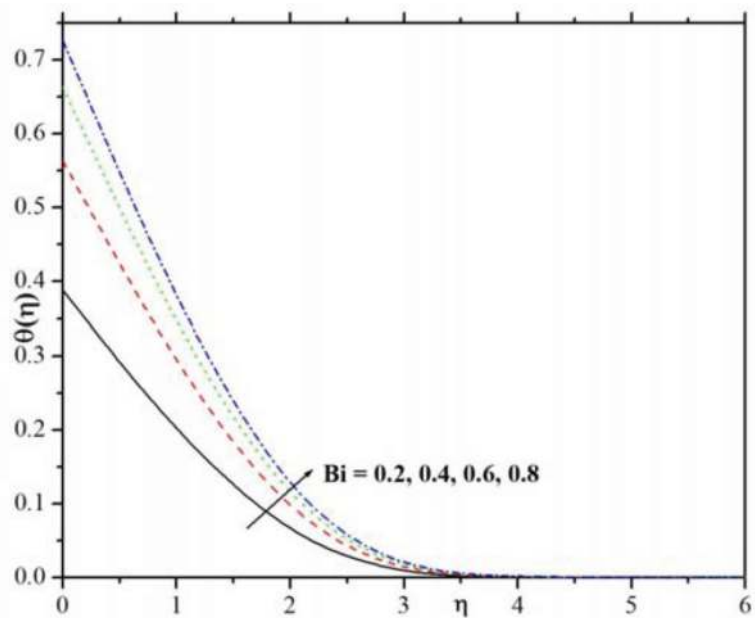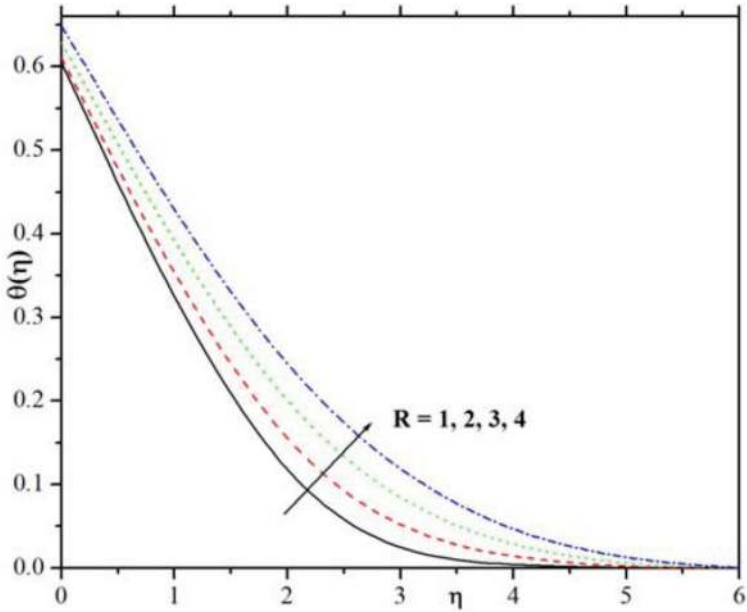

Figure 7. Influence of Bi on temperature profile.

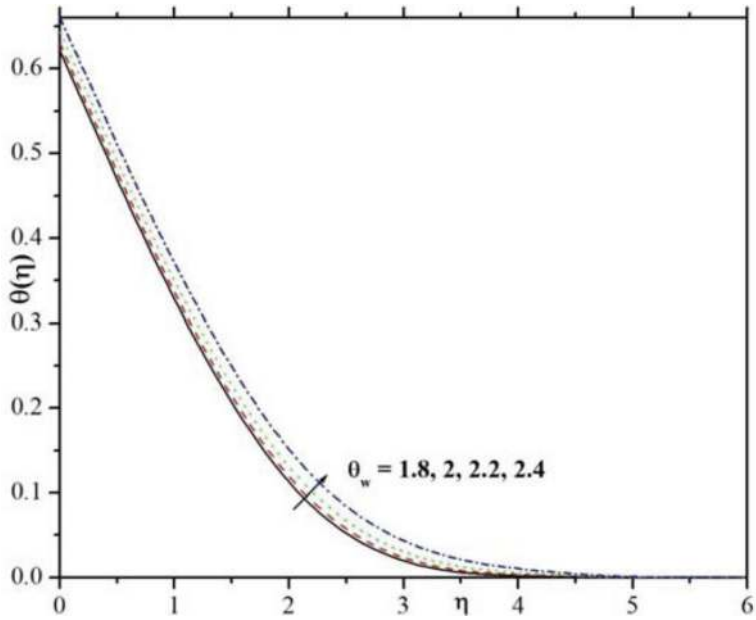**Figure 8.** Influence of R on temperature profile.

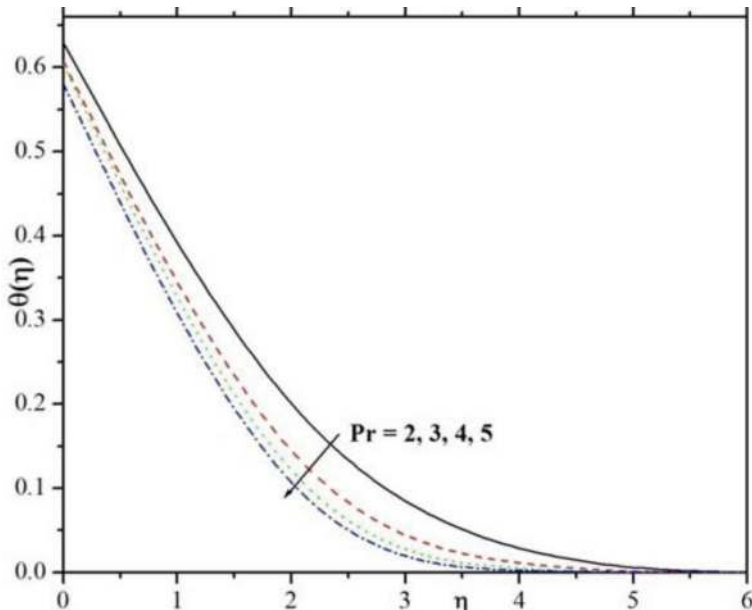**Figure 9.** Influence of θ_w on temperature profile.

Figure 10. Influence of Pr on temperature profile.

Figure 1 characterizes the influence of Weissenberg number (We) on velocity profiles for both x and y direction. It is found that increasing values of the Weissenberg number increases the momentum boundary layers in both directions. Physically, Weissenberg number is directly proportional to the time constant and reciprocally proportional to the body. The time constant to body magnitude relation is higher for larger values of Weissenberg number. Hence, higher Weissenberg number causes to enhance the momentum boundary layer thickness.

The developments of a magnetic field (M) on velocity profiles are circulated in **Figure 2**. We tend to discover depreciation within the velocity profile for ascent values of magnetic field parameter. Physically, the drag force will increase with a rise within the magnetic flux and as a result, depreciation happens within the velocity field.

Figure 3 designed the velocity profiles of f' and g' for various values of stretching parameter(c). The velocity profiles and associated momentum boundary layer thickness decrease, once the stretching parameter will increase whereas velocity profile g', exhibits the opposite behavior of f'. **Figure 4** shows the velocity profiles for different values of mixed convection parameter(λ). It depicts that the velocity field and momentum boundary layer thickness increases in both x and y direction by increasing mixed convection parameter.

Figure 5 portraits the consequences of Brownian motion parameter on temperature and concentration profile. The Brownian motion parameter (Nb) will increase the random motion of the fluid particles and thermal boundary layer thickness conjointly will increase which ends up
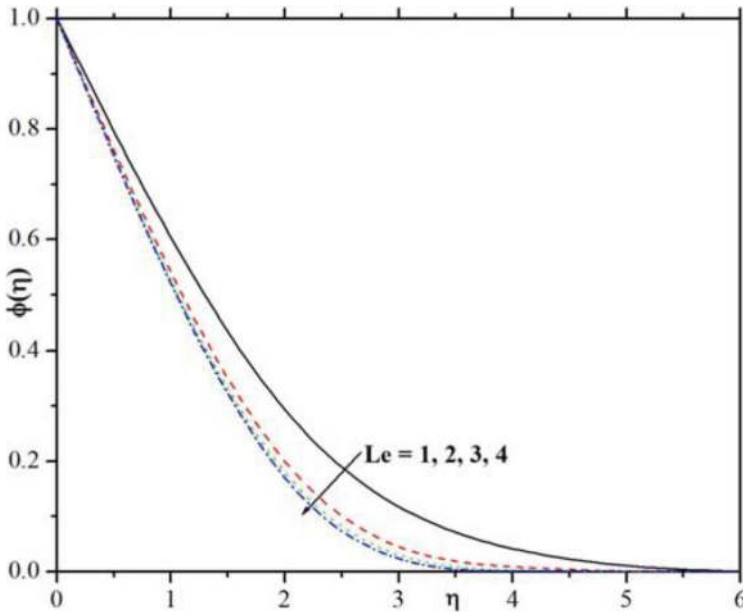
Figure 11. Influence of *Le* on concentration profile.

in an additional heat to provide. Therefore, temperature profile will increase however concentration profiles show opposite behavior.

The development of the thermophoresis parameter (Nt) on temperature and concentration profiles is inspecting in **Figure 6**. Form this figure we observed that, the higher values of thermophoresis parameter is to increases both $\theta(\eta)$ and $\phi(\eta)$ profiles. Further, the thermal boundary layer thickness is higher for larger values of thermophoresis parameter. This is because, it's a mechanism within which little particles area unit force off from the new surface to a chilly one. As a result, it maximizes the temperature and concentration of the fluid.

Figure 7 describe the influences of Biot number (Bi) on temperature profile. One can observe form the figure, the larger values of Biot number cause an enhancing the temperature profile. This is because, the stronger convection leads to the maximum surface temperatures which appreciably enhance the thermal boundary layer thickness.

Figures 8 and **9** are sketched to analyze the effect of radiation parameter (R) and temperature ratio (θ_w) parameter on temperature profile. The above graphs elucidate that, the temperature profile and thermal boundary layer thickness area unit increased by ascent values of radiation parameter and temperature ratio. Larger values of thermal radiation parameter provide more heat to working fluid that shows an enhancement in the temperature and thermal boundary layer thickness.

The effect of the Prandtl number (Pr) on $\theta(\eta)$ is seen in **Figure 10**. Since Pr is that the magnitude relation of the viscous diffusion rate to the thermal diffusion rate, the upper worth

Bi	Le	R	c	λ	M	Absence		Presence	
						C_{fx}	C_{fy}	C_{fx}	C_{fy}
0.2						1.2240	0.7261	1.3030	0.7836
0.4						1.1795	0.7280	1.2642	0.7847
0.6						1.1532	0.7289	1.2412	0.7854
	2					1.1719	0.7283	1.2575	0.7850
	3					1.1648	0.7285	1.2514	0.7851
	4					1.1619	0.7285	1.2489	0.7851
		1				1.1598	0.7289	1.2466	0.7855
		2				1.1420	0.7301	1.2300	0.7866
		3				1.1220	0.7314	1.2113	0.7878
			0.2			1.0852	0.2066	1.1657	0.2083
			0.4			1.1265	0.4509	1.2096	0.4657
			0.6			1.1648	0.7285	1.2514	0.7851
				0		1.3122	0.7242	1.3787	0.7816
				0.2		1.2523	0.7259	1.3143	0.7834
				0.4		1.1936	0.7276	1.2514	0.7851
					0	0.9611	0.5965	1.0281	0.6293
					0.5	1.1648	0.7285	1.2514	0.7851
					1	1.3441	0.8413	1.4521	0.9248

Table 2. Numerical result of skin friction coefficient for different physical parameter values for present and absence non Newtonian fluid.

of Prandtl number causes to scale back the thermal diffusivity. Consequently, for increasing values ofPr, the temperature profile gets decreases. The impact of Lewis number (Le) on nanoparticle concentration is plotted in **Figure 11**. It is evident that the larger values of Lewis number cause a reduction in nanoparticles concentration distribution. Lewis number depends on the Brownian diffusion coefficient. Higher Lewis number leads to the lower Brownian diffusion coefficient, which shows a weaker nanoparticle concentration.

Table 2 presents the numerical values of skin friction for various physical values in the presence and absence ($We = n = 0$) of non-Newtonian fluid. It is observed that skin friction increase in both directions with increasing c for both presence and absence of non-Newtonian fluid. In the other hand, the skin friction coefficient decreases in both directions by increasingBi. The skin friction is higher in the presence of non-Newtonian fluid than in the absence of non-Newtonian fluid.

Table 3 also elucidates that, the wall temperature for different physical parameter for linear as well as nonlinear radiation. It reveals that, the wall temperature increases for increasing values of Bi, R and c for both linear and nonlinear radiation but the wall temperature decreases by

Bi	Le	M	Nb	R	Nt	Pr	c	Linear $-Nu_x(\mathbf{Re}_x)^{-1/2}$	Nonlinear $-Nu_x(\mathbf{Re}_x)^{-1/2}$
0.2								0.1060	0.3289
0.4								0.1356	0.4683
0.6								0.1479	0.5421
	2							0.1825	0.5501
	3							0.1428	0.5102
	4							0.1200	0.4886
		0						0.1440	0.5206
		0.5						0.1428	0.5102
		1						0.1418	0.5011
			0.2					0.3354	0.8074
			0.4					0.2771	0.6974
			0.6					0.2091	0.5974
				1				0.1768	0.8621
				2				0.2059	1.5030
				3				0.2150	2.0523
					0			0.1834	0.5641
					0.5			0.1331	0.4971
					1			0.0913	0.4351
						2		0.2165	0.4958
						3		0.2059	0.5260
						4		0.1875	0.5307
							0.2	0.1268	0.4606
							0.4	0.1352	0.4870
							0.6	0.1428	0.5102

Table 3. Numerical result of Nusselt number for different physical parameter values for linear and non nonlinear radiation.

increasing Le, Nb, Nt and Pr. Further, it is noticed that the wall temperature is higher for nonlinear radiation than that linear radiation.

Table 4 clearly shows the numerical values of skin friction, Nusselt number and Sherwood number for various physical parameters values. It reveals that, numerical values of wall temperature $\theta(0)$ increase by increasing Bi, θ_w, R and c. In the other hand Nusselt number decreases by increasing. Le, M, Nb, Nt and Pr. From this table, the skin friction coefficient increases by increasing Bi and m. Further, the Sherwood number increases by increasing Bi, θ_w, R, Pr and We.

Bi	θ_w	Le	M	Nb	R	Nt	Pr	We	c	λ	$-C_{fx}$	$-C_{fy}$	$-Sh_x(\mathrm{Re}_x)^{-\frac{1}{2}}$	$-Nu_x(\mathrm{Re}_x)^{-\frac{1}{2}}$
0.2											1.3030	0.7836	1.4859	0.3289
0.4											1.2642	0.7847	1.4877	0.4683
0.6											1.2412	0.7854	1.4886	0.5421
	1.8										1.2434	0.7856	1.4825	0.7398
	2										1.2353	0.7860	1.4812	0.9218
	2.2										1.2250	0.7865	1.4814	1.1226
		2									1.2575	0.7850	1.1427	0.5501
		3									1.2514	0.7851	1.4882	0.5102
		4									1.2489	0.7851	1.7744	0.4886
			0								1.0281	0.6293	1.5340	0.5206
			0.5								1.2514	0.7851	1.4882	0.5102
			1								1.4521	0.9248	1.4493	0.5011
				0.2							1.3140	0.7831	1.2408	0.8074
				0.4							1.2926	0.7837	1.4118	0.6974
				0.6							1.2713	0.7844	1.4647	0.5974
					1						1.2466	0.7855	1.4781	0.8621
					2						1.2300	0.7866	1.4727	1.5030
					3						1.2113	0.7878	1.4740	2.0523
						0					1.2674	0.7845	1.4869	0.5641
						0.5					1.2472	0.7853	1.4901	0.4971
						1					1.2255	0.7863	1.5060	0.4351
							2				1.2113	0.7878	1.4740	0.4958
							3				1.2345	0.7863	1.4731	0.5260
							4				1.2449	0.7857	1.4767	0.5307
								0			1.1936	0.7276	1.4746	0.5070
								1			1.2974	0.8329	1.4985	0.5127
								2			1.3712	0.9109	1.5141	0.5164
									0.2		1.1657	0.2083	1.2770	0.4606
									0.4		1.2096	0.4657	1.3862	0.4870
									0.6		1.2514	0.7851	1.4882	0.5102
										0	1.3787	0.7816	1.4738	0.5068
										0.2	1.3143	0.7834	1.4811	0.5085
										0.4	1.2514	0.7851	1.4882	0.5102

Table 4. Numerical result of local skin friction coefficient, Sherwood number and Nusselt number for different physical parameter.

5. Conclusions

In the present study, influence of nonlinear radiation on three dimensional flow of an incompressible non-Newtonian Carreau nanofluid has been obtained. The obtained results are presented in tabulated and graphical form with relevant discussion and the Major findings from this study are:

The velocity profiles increase in $x-$ directions and decrease in the $y-$ direction by increasing the stretching parameter.

Concentration profile increase by increasing the values Nb but in case of Nt concentration profile decreases.

Nb and Nt parameter shows the increasing behavior for temperature profile.

Effects of Le nanoparticle fraction $\phi(\eta)$ show the decreasing behavior.

Magnetic parameter reduces the velocity profiles in both x and $y-$ directions.

Temperature and thermal boundary layer thickness are decreased when the Pr and tl number increases.

Nonlinear thermal radiation should be kept low to use it as a coolant factor.

The rate of heat transfer increases with the increases in parameters Rd and θ_w.

We also noticed that the velocity profile and its associated boundary layer thickness are increases by increasing the values of We.

Author details

Rudraswamy N.G.[1]*, Ganeshkumar K.[2], Krishnamurthy M.R.[3], Gireesha B.J.[2] and Venkatesh P.[1]

*Address all correspondence to: ngrudraswamy@gmail.com

1 Department of Mathematics, Sahyadri Science College (Autonomous), Kuvempu University, Shimoga, India

2 Department of P.G. Studies and Research in Mathematics, Kuvempu University, Shankaraghatta, India

3 Department of Mathematics, JNN College of Engineering, Shivamogga, India

References

[1] Anwar Bég O, Ghosh SK, Narahari M, Bég TA. Mathematical modelling of thermal radiation effects on transient gravity-driven optically-thick gray convection flow along

an inclined plate with pressure gradient. Chemical Engineering Communications. 2011;
198:1-15

[2] Rahman MM, Eltayeb IA. Radiative heat transfer in a hydromagnetic nanofluid past a non-linear stretching surface with convective boundary condition. Meccanica. 2013;**48**:601-615

[3] Rashidi MM, Ganesh NV, Abdul Hakeem AK, Ganga B. Buoyancy effect on MHD flow of nanofluid over a stretching sheet in the presence of thermal radiation. Journal of Molecular Liquids. October 2014;**198**:234-238

[4] Srinivas S, Muthuraj R. Effects of thermal radiation and space porosity on MHD mixed convection flow in a vertical channel using homotopy analysis method. Communications in Nonlinear Science and Numerical Simulation. 2010;**15**:2098-2108

[5] Zeeshan A, Majeed A, Ellahi R. Effect of magnetic dipole on viscous ferro-fluid past a stretching surface with thermal radiation. Journal of Molecular Liquids. 2016;**215**:549-554

[6] Cortell R. Fluid flow and radiative nonlinear heat transfer over stretching sheet. Journal of King Saud University Science. 2013;**26**:161-167

[7] Ferdows M, Khan MS, Anwar Bég O, Azad MAK, Alam MM. Numerical study of transient magnetohydrodynamic radiative free convection nanofluid flow from a stretching permeable surface. Proceedings of Institution of Mechanical E-Part E: Journal of Process Mechanical Engineering. 2014;**228**(3):181-196

[8] Anwar Bég O, Ferdows M, Bég A, Tasveer T, Ahmed MW, Alam MM. Radiative optically-dense magnetized transient reactive transport phenomena with cross diffusion and dissipation effects. Numer. Simul. Journal of Taiwan Institute of Chemical Engineers. 2016:15

[9] Pal D, Mondal H. Effects of Soret Dufour, chemical reaction and thermal radiation on MHD non-Darcy unsteady mixed convective heat and mass transfer over a stretching sheet. Communications in Nonlinear Science and Numerical Simulation. 2011;**16**(4):1942-1958

[10] Murthy PVSN, Mukherjee S, Srinivasacharya D. Combined radiation and mixed convection from a vertical wall with suction/injection in a non–Darcy porous medium. Acta Mechanica. 2004;**168**(3–4):145

[11] Sheikholeslami M, Ganji DD, Javed MY, Ellahi R. Effect of thermal radiation on magneto-hydrodynamics nanofluid flow and heat transfer by means of two phase model. Journal of Magnetism and Magnetic Materials. 2015;**374**:36-43

[12] S. Snyder, N. Arockiam, P.E. Sojka, Secondary Atomization of Elastic Non-Newtonian Liquid Drops, In: AIAA Joint Propulsion Conference, Nashville, Tennessee, USA, 2010

[13] Kumar KG, Gireesha BJ, Rudraswamy NG, Gorla RSR. Melting heat transfer of hyperbolic tangent fluid over a stretching sheet with fluid particle suspension and thermal radiation. Communications in Numerical Analysis. 2017;**2017**(2):125-140

[14] Cortell R. Effects of viscous dissipation and radiation on the thermal boundary layer over a nonlinearly stretching sheet. Physical Letters A. 2008;**372**(5):631-636

[15] Batalle RC. Viscoelastic fluid flow and heat transfer over a stretching sheet under the effects of a non-uniform heat source, viscous dissipation and thermal radiation. International Journal of Heat and Mass Transfer. 2007;**50**(15–16):3152-3162

[16] Khan M, Hussain M, Azam M. Magnetohydrodynamic flow of Carreau fluid over a convectively heated surface in the presence of non-linear radiation. JMMM. 2016;**412**:63-68

[17] Khan MI, Alsaedi A, Shehzad SA, Hayat T. Hydromagnetic nonlinear thermally radiative nanoliquid flow with Newtonian heat and mass conditions. Results Physics. 2017;**7**:2255-2260

[18] Rana P, Bhargava R. Numerical study of heat transfer enhancement in mixed convection flow along a vertical plate with heat source/sink utilizing nanofluids. Communication in Nonlinear Science Numerical Simulation. 2011;**16**(11):4318-4334

[19] Hayat T, Shehzad SA, Alsaedi A, Alhothuali MS. Mixed convection stagnation point flow of Casson fluid with convective boundary conditions. Chinese Physics Letters. 2012;**29**(11):114704. https://doi.org/10.1088/0256-307X/29/11/114704

[20] Laxmi T, Shankar B. Effect of nonlinear thermal radiation on boundary layer flow of viscous fluid over nonlinear stretching sheet with injection/suction. Journal of Applied Mathematical Physics. 2016;**4**:307-319

[21] Kumar KG, Rudraswamy NG, Gireesha BJ, Manjunatha S. Non-linear thermal radiation effect on Williamson fluid with particle-liquid suspension past a stretching surface. Results in Physics. 2017;**7**:3196-3202

[22] Kumar KG, Gireesha BJ, Manjunatha S, Rudraswamy NG. Effect of nonlinear thermal radiation on double-diffusive mixed convection boundary layer flow of viscoelastic nanofluid over a stretching sheet. International Journal of Mechanical Material Engineering. 2017;**12**(1):18

[23] Mabood F, Imtiaz M, Alsaedi A, Hayat T. Unsteady convective boundary layer flow of Maxwell fluid with nonlinear thermal radiation: A numerical study. International Journal of Nonlinear Science Numerical Simulation. 2016;**17**(5):221-229

[24] Shehzad SA, Hayat T, Alsaedi A, Obid MA. Nonlinear thermal radiation in three-dimensional flow of Jeffrey nanofluid: A model for solar energy. Applied Mathematics and Computation. 2016;**248**:273-286

[25] Hayat T, Muhammad T, Alsaedi A, Alhuthali MS. Magnetohydrodynamic three-dimensional flow of viscoelastic nanofluid in the presence of nonlinear thermal radiation. JMMM. 2015;**385**:222-229

[26] Rudraswamy NG, Kumar KG, Gireesha BJ, Gorla RSR. Soret and Dufour effects in three-dimensional flow of Jeffery nanofluid in the presence of nonlinear thermal radiation. Journal of Nanoengineering Nanomanufacturing. 2016;**6**(4):278-287

[27] Wang CY. The three-dimensional flow due to a stretching sheet. Physics of Fluids. 1984;**27**:1915-1917

[28] Hayat T, Muhammad T, Shehzad SA, Alsaedi A. Similarity solution to three dimensional boundary layer flow of second grade nanofluid past a stretching surface with thermal radiation and heat source/sink. AIP Advances. 2015;**5**:017107. https://doi.org/10.1063/1.4905780

[29] Shehzad SA, Hayat T, Alsaedi A. MHD three dimensional flow of viscoelastic fluid with thermal radiation and variable thermal conductivity. A Journal of Central South University. 2014;**21**(10):3911-3917

[30] Hayat T, Shehzad SA, Alsaedi A. Three-dimensional stretched flow of Jeffrey fluid with variable thermal conductivity and thermal radiation. Applied Mathematics and Mechanics. 2013;**34**:823-832